Hindawi
Journal of Engineering
Volume 2022, Article ID 5490585, 13 pages
https://doi.org/10.1155/2022/5490585

Research Article

Analysis of Three-Wheeler Vehicle Structure at the Event of Side Pole Crash

Daniel Hambissa,[1] Ramesh Babu Nallamothu ,[2] and Tigist Andarge[2]

[1]*Department of Mechanical Engineering, Wolkite University, Wolkite, Ethiopia*
[2]*Department of Mechanical Engineering, Adama Science and Technology University, Nazareth, Ethiopia*

Correspondence should be addressed to Ramesh Babu Nallamothu; rbnallamothu@gmail.com

Received 17 March 2022; Accepted 31 May 2022; Published 29 June 2022

Academic Editor: Francesco Colangelo

This work reports on the simulation of three-wheel vehicles in the event of a side pole crash. In this study, the dynamic characteristics of the three-wheeler vehicle during pole collision were studied using finite elements. The TWV model used here was created using CATIA v5 and simulated using LS-DYNA which is widely used by the automotive industry to analyze vehicle design and predict a car's behavior in a collision. Moreover, in this study, the finite element model of the side hybrid 5th percentile male dummy was developed for studying the driver and occupant responses in crash events of side pole. Based on the analysis results obtained from the existing model of TWV, modifications were made on the side structure by means of adding energy-absorbing components. Then, the modified TWV was analyzed under the same condition as the existing one. The result of the simulations shows that with the modification, 80 mm more living space, 630 N reduction of impact force, and 0.8 kJ of additional absorbed energy were obtained. So with the modified model, the safety and crashworthiness of the TWV were greatly improved during side collision without affecting the appearance and weight of the existing models.

1. Introduction

In all countries, the rate of vehicle side collisions is high. Protection of occupants is very difficult on side collisions due to lack of sufficient space for large deformation, so side impacts are very dangerous. In vehicles collisions, in terms of causes of death, side impact collision is occupying the second position just after frontal collision in the USA [1]. The collision of vehicles on the side with a pole or tree remains the most dangerous collision event. From 2004 to 2009, the fatalities mounted to 52% in track side crash against a rigid pole as per statistical data, where the share of a side impact is more than 60% [2].

The titles related to energy absorption side structure of vehicles and responses of humans in the event of side impact are very much researched to take countermeasures against the dangerous side impact [3]. This paper focuses on the dynamic characteristics of the three-wheeler vehicle during pole collision using finite elements. A three-wheel vehicle (TWV) is shown in Figure 1. It generally has rear two wheels, front one wheel, with open frame and body mode of sheet metal. The driver generally sits at the front in a small cabin, and there is a place in the rear of the vehicle for the passengers to sit. On the front side, the headlamp is attached to the mudguard, windscreen on the upright body, and canvas roof. 55 km/hr is the maximum velocity of the vehicle. The total weight of the vehicle is around 650 kg including the driver and three passengers [5].

The crashworthiness of three wheelers is not evaluated except for some basic safety features. The regulations of vehicle crashes were mostly developed for cars other than TWV [5]. Three-wheeler vehicle side crashes are the most dangerous accidents because of the existence of less space between the pole and occupants. Since the three-wheeler vehicle is manufactured with open design without side doors, the open space will produce more severe conditions for the occupants in case of an accident. Moreover, this vehicle has no side protection or energy-absorbing system,

Figure 1: Three-wheeler structure.

and the worst case will happen to the occupants due to large structural deformation because of the small contact area in crash with trees.

This paper aimed to solve and improve the side crashworthiness of the existing three-wheeled vehicles. Therefore, the first task carried out in this paper was modeling and analysis of the existing three-wheeled vehicle structure. Based on the interpretation of the results obtained, the structure of existing three-wheeled vehicles is modified. For accomplishing this task, software like CATIA v5 was used for modeling, and LS-DYNA was used for FEA analysis.

1.1. Side Impact Test Standard

1.1.1. FMVSS 214 and IIHS Standard. Nowadays, to minimize the injuries and death of vehicle occupants during a side collision, there are several vehicle crash test standards that help vehicle manufacturers to improve the safety of their vehicle products. Among the existing standards, Federal Motor Vehicle Safety started to implement standard for side impact protection (FMVSS 214) in 1990. In addition, in 1997, a Moving Deformable Barrier (MDB) was introduced by National Highway Traffic Safety Administration (NHTSA) for the testing crash in a side impact. The MDB has mass of 1368 kg, with a velocity of 54 km/h, striking a stationary vehicle at a 90° angle with a crabbed wheel angle of 27°; see Figure 2(a). When measured from the ground, the height of the part of the barrier which deforms is 828 mm [6]. This helps to figure out what could happen if a car side crashed at an intersection. In 2003, Insurance Institute for Highway Safety (IIHS) starts to test vehicle side impact using modified MDB as shown in Figure 2(b). In this test, the modified MDB weighs 1500 kg, moves with 50 km/h, and then hits the stationary vehicle on the driver side. The dimension of IIHS MDB is equal to a typical midsize SUV [6].

1.1.2. Lateral NCAP Pole Test. The simulation of this test helps in understanding the consequences of a driver sliding off a road crashing with a utility pole. In the NHTSA and IIHS crash test safety ratings, a vehicle in the NCAP side pole test is sent into a fixed, rigid pole 254 mm (10 inches) in diameter, at a speed of 32 km/h (20 mph); see Figure 3. For this study, the same settings were applied for examining the side crashworthiness of the TWV. The details of the implemented standard are shown in Section 2.7.

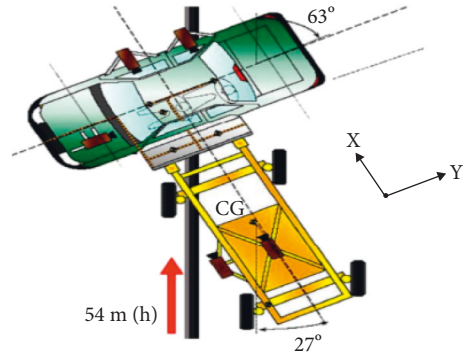

Figure 2: A FMVSS side impact test.

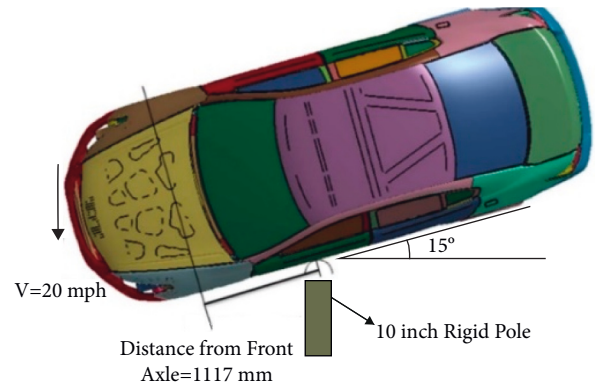

Figure 3: NACP side impact test.

Not much research has been done on TWV, autorickshaws in particular. FEA software was used to analyze the strength of the structure of TWV in rollover static, rear, frontal, and side impacts. Based on the obtained result from the existing model, a modified model of TWV was proposed by making some changes to the structure. The result showed that the modified model is much better than the existing model, but the research work did not consider the dynamic crash event. It only focuses on a static basis [7, 8]. The safety of TWV occupants is less as compared to other vehicles. Most of the time, the event of front crashing causes thorax, head, and knee injuries to the occupants, which are areas of concern, so with low-cost changes to interiors of the TWV, the severity of injuries can be minimized [9]. Otherwise, occupants can sustain high HICs, face/head contact forces, and tibia/knee contact forces in crashes with buses at velocities of 20 km/h and greater [10]. In addition to the occupants, the TWV structure can cause serious injury to pedestrians [11]. There is no front bumper for the TWV and hence no frontal energy-absorbing member. The injuries that occur to the occupants during frontal impact are more when compared to those during rear impact. The rear crash modulus is much higher than that of the frontal crash [12]. In addition to the occupant and passenger safety, the side structure of the TWV should be modified for the dynamic crash events by adding some bumper or energy-absorbing unit. This paper aimed to improve or modify the TWV structure in the event of side crashes.

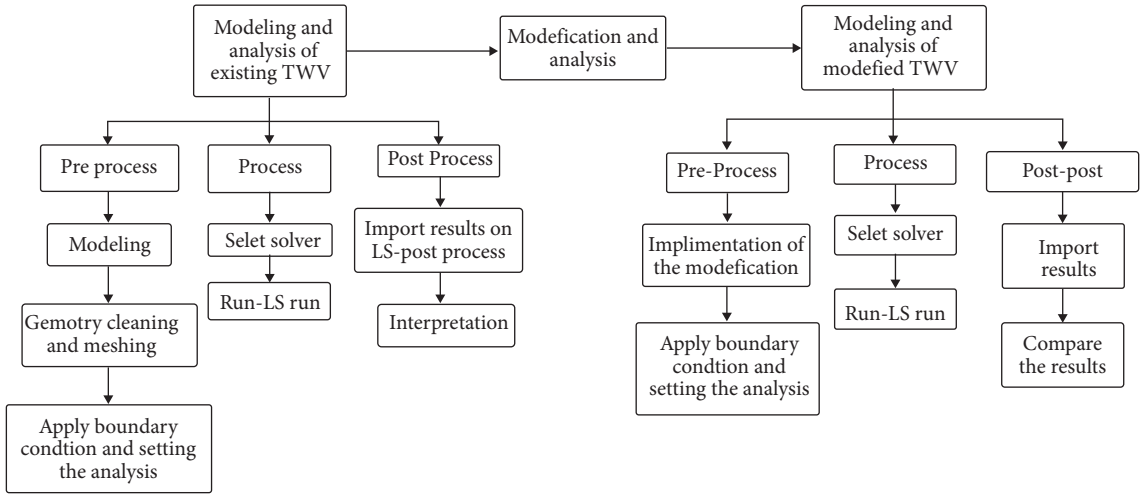

Figure 4: FEA methodology.

Figure 5: 3D modeling of TWV.

Figure 6: Meshed TWV.

2. Materials and Methods

In performing the analysis and modeling of the side crashworthiness of the three-wheeled vehicle, the steps followed are listed in Figure 4.

2.1. Modeling of Existing TWV. The geometry model of three-wheeled vehicle is created based on specifications obtained from data collection [8, 11]. The parts were modeled separately and assembled in CATIA. The main modeled parts were the front and rear body structure, steering, wind screen, roof, front and rear tyres, main frames, and seat foams. The assembled 3D modeling of the three-wheeled structure is shown in Figure 5.

2.2. Mesh Generation. When considering the structure of TWV, the thicknesses of the main components is much less than the length and width, so a shell element is used for modeling. Therefore, a 2D mesh type was used. The three-wheel vehicle geometry was meshed by LS-DYNA software by mixing linear quadrilateral (97.7%) and triangular elements (0.295%). The element size for the whole model is between 2 mm and 6 mm. The meshed model consists of 1292983 elements and 1311326 nodes. The meshed TWV is shown in Figure 6.

2.3. Part Material Properties and Thicknesses of the TWV Components. LS-DYNA material library is used for the selection of materials for vehicle components. The keyword used for the tire was modeled by MAT_ELASTIC, while the windscreen and vehicle structures were modeled by MAT_PIECEWISE_LINEAR_PLASTICITY. The roof was modeled by MAT_FABRIC. Since some parts are not subjected to deformation, they were modeled by MAT_RIGID; these are seat, axle, and engine component representation. The mechanical properties and thickness of the shell of the vehicle components are given in Tables 1 and 2.

Section shell is used for defining the thickness of most vehicle components, and the rest were defined with solid elements. For shell elements, the value of the thickness is determined based on their density and mass value listed on the above data collections.

2.4. Contact Definition. The contact between two parts is given to prevent penetration during the crash. There are a lot of contact types available in the Keyword Manager. The contact types used in this paper are shown in Table 3.

2.5. The Occupant Restraint System. The TWV is equipped with a 5^{th} percentile hybrid side dummy. Therefore, the occupant motion and contact area inside the TWV vehicle can be

Table 1: Mechanical properties of the vehicle component.

Vehicle item	Mass density (kg/mm^3)	Young's modulus (kN/mm^3)	Poisson's ratio	Yield stress (kN/mm^3)	Shear modulus (kN/mm^3)	Tangent modulus
Vehicle structure	7.80e−006	210	0.3	0.25		1
Chassis and roof support	7.80e−006	210	0.3	0.25		
Windscreen	2.500e−006	76	0.3	0.138		1
Roof	6.800e−006	135	0.35		5	
Seat (cushion)	1.010e−007	0.00416	0.35			
Tire	1.700e−006	24.61	0.32			

Table 2: Thicknesses of the vehicle components.

Vehicle component	Thicknesses (mm)
Vehicle structure	1
Seat (cushion)	0.5
Frame or chassis	6
Roof support	2
Roof	0.15
Windscreen	3
Tire	5

Table 3: Contact between different parts of TWV.

Contact type	Slave	Master
Automatic surface to surface	Tire	Ground
Automatic surface to surface	TWV	Pole
Automatic single surface	Whole vehicle	None

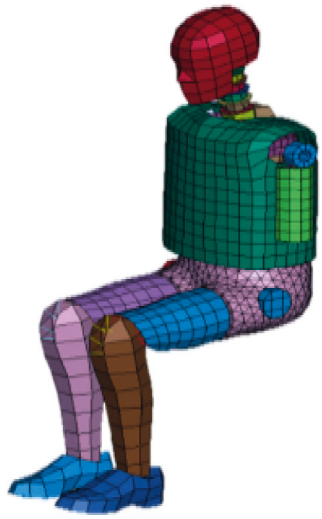

Figure 7: Side dummy.

seen. The dummy is shown in Figure 7. The TWV is equipped with two side dummies to observe the occupant's motion. The first one is used to indicate the driver position whereas the other is positioned inside the passenger's compartment.

2.6. Missing Components and Simplifying the Model. To minimize the computer simulation time, model simplification was necessary; thus, among passenger dummies, only the right side dummy was considered, and other vehicle parts were not modeled. However, for considering the mass of the occupants and TWV, the center of gravity is measured, and the sum of their mass is applied at that point.

2.7. Missing Components and Simplifying the Model. To minimize the computer simulation time, model simplification was necessary; thus, among passenger dummies, only the right side dummy was considered, and other vehicle parts were not modeled. However, for considering the mass of the occupants and TWV, the center of gravity is measured and the sum of their mass is applied at that point.

2.8. Boundary Condition. Here, as is mentioned in a previous section, boundary condition in accordance with lateral NCAP pole test standard is implemented on TWV. To analyze the real crash event of TWV hitting a pole or tree, we set up FEA model in which the three-wheeler vehicle moves with a velocity of 25 km/h and then strikes the rigid pole at an angle of 75° with the vehicle's longitudinal axis adjusted. The rigid pole used for the simulation can be downloaded from NHTSA website [13]. According to the standard, the diameter of the rigid pole is 254 mm and it is arranged vertically with the following:

(i) Maximum 102 mm above the end of the TWV tires

(ii) Extended 150 mm above the roof of TWV

(iii) The direction of vehicle motion being such that the pole is always aligned with the CG of the head of the driver [14]

The LS-DYNA setup of side crashworthiness test TWV model as per NACP regulation is shown in Figures 8(a) and 8(b).

2.9. Modification in the Existing Three-Wheeler Vehicle. To reduce the force of impact transferred to the occupants and minimize intrusion into the compartments at the event of side crashes, deformable side beam elements are mounted at the frame structure of TWV. The location in which the modification was fitted is shown in Figure 9.

2.10. Side Bumper Beam Design. Side beam is considered as one of the important safety components which strengthen the

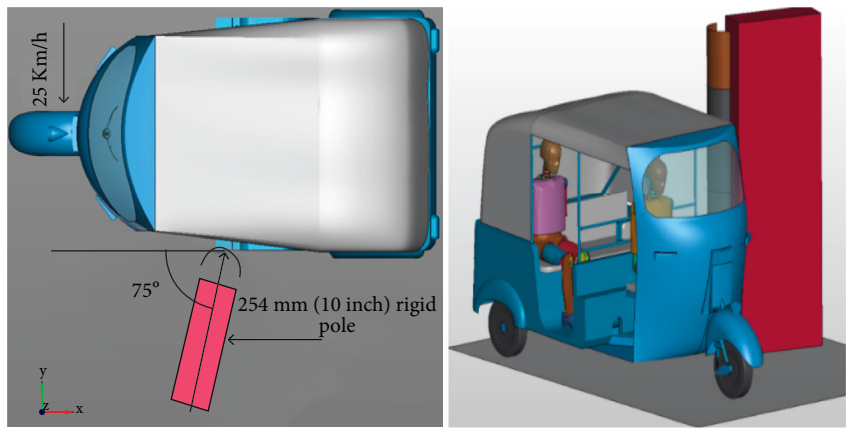

Figure 8: Side test setup.

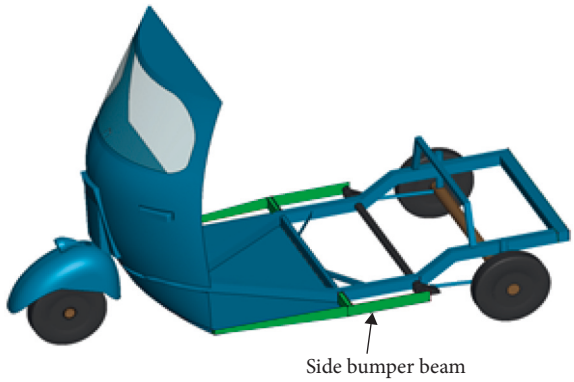

Figure 9: Modified TWV.

side members of the TWV and help in lowering the degree of injures to occupants during a side collision. Under this section, a bumper beam with carbon fibre composite unidirectional IM7/8552 material is designed for different thicknesses.

A rectangular cross section is used for the bumper beam having maximum bending stiffness to other cross-sections as suggested by [15]. The use of lightweight material especially for three-wheeler vehicle provides opportunities for reducing vehicle weight, thus increasing fuel efficiency and reducing the emission of harmful pollutants. So, for the bumper beams, carbon fibre composite material is taken into consideration to achieve the required performance [16]. The data related to material properties are obtained from the literature [17]. The data obtained from the literature were used directly as physical parameters in LS-DYNA material cards, and they are summarized in Table 4.

2.11. Material, Thickness, and Boundary Definition. The material keyword used to define the material is*MAT_ENHANCED_COMPOSITE_DAMAGE or*MAT_054 or *MAT_055 [18]. A shell section is employed to model the bumper beam since its thickness is thought to be quite tiny in comparison to its entire length. The shell elements are formulated by ELFORM = 2 (Belytschko-Tsay elements). In LS-DYNA, this can be set by user input card *SECTION_SHELL/_TSHELL [19]. Rectangular cross-

Table 4: Side beam composite material property.

Properties	Units	Values
Mass density, ρ	kg/mm^3	1.58E−06
Young's modulus, E_{11}	MPa	165000
Young's modulus, E_{22}	MPa	9000
Poisson's ratio (minor), μ_{12}/μ_{13}	—	0.0185
Poisson's ratio, μ_{23}	—	0.5
Shear modulus, G_{12}/G_{31}	MPa	5600
Shear modulus, G_{23}	MPa	2800
Longitudinal compressive strength, XC	MPa	1590
Longitudinal tensile strength, XT	MPa	2560
Transverse compressive strength, YC	MPa	185
Transverse tensile strength, YT	MPa	73
Shear strength, SL	MPa	90
Strain at longitudinal compressive strength, $\in_{11C}$	—	0.011
Strain at longitudinal tensile strength, $\in_{11T}$	—	0.01551
Strain at transverse compressive strength, $\in_{22C}$	—	0.032
Strain at transverse tensile strength, $\in_{22T}$	—	0.0081
Engineering strain at shear strength, γ_{12S}	—	0.05

sections with different thicknesses of carbon fibre composite bumper beam are taken into consideration to achieve the effect of thickness on the impact performance of the bumper system. A good bumper beam is one that has seven layers with fiber orientations of [0, ±30, ±60, and 90] [20]. The thickness of the side bumper beam that was considered is 4.5, 5, 5.5, 6, 6.5, and 7.2 mm. The reason for starting from 4.5 mm thickness is that when the material thickness was as low as this value, it showed some kind of faller mode.

Among the listed ones, the best material thickness is selected based on parameters like load carrying capacity, stress energy absorption capacity, and reduction in displacement.

The boundary conditions and the setups used are shown in Figure 10. The test consists of three components; these are the supports (red color), bumper beam (blue), and rigid pole (black). The pole is represented by a rigid body and discretized by solid elements. The beam and its supports utilize a single-layered modeling approach, where only one layer of shell elements (because the thickness of the bumper beam is much

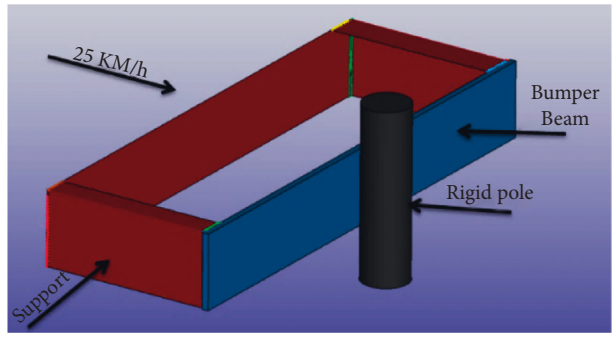

Figure 10: Side beam test.

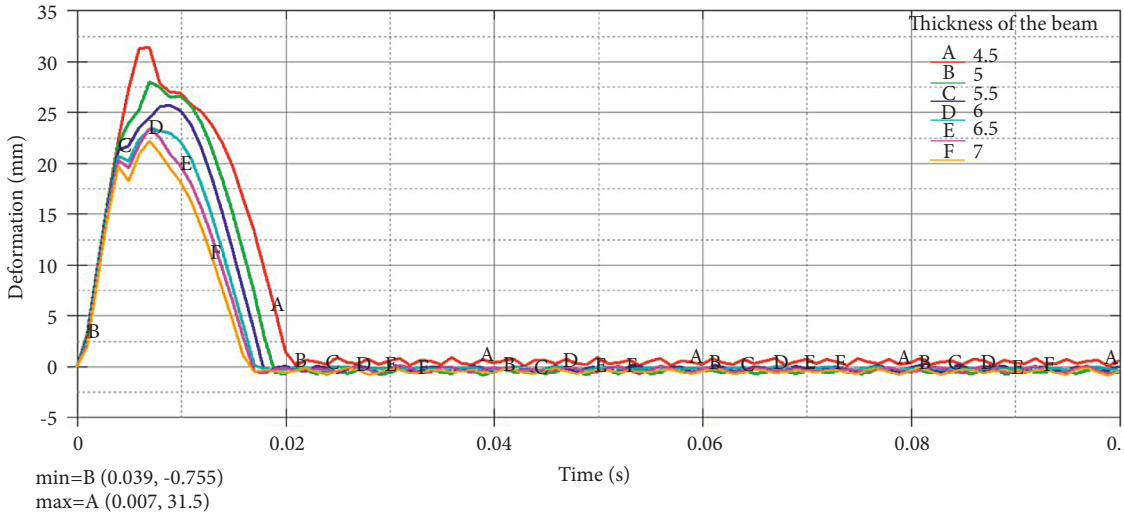

Figure 11: Deformation of different beam thicknesses.

smaller than the other dimensions) is implemented for efficiency. The components are mainly mashed with quadrilateral elements with fewer triangular ones and consist of 18199 elements and 19430 nodes. MAT 20 (mat-rigid) is used for simulation of the rigid pole, and MAT 24 (MAT_PIECEWISE_LINEAR_PLASTICITY) is used for the supports of the beams. The test procedure follows the same procedure used in the full crash test of the TWV. The supports were arranged or set up in the same manner as the point where the modification was made on TWV.

The same distance that was set between the TWV and rigid pole was also set for the bumper beam and the side pole. The support together with the bumper beam moving with 25 km/h was collided with the rigid pole; see Figure 10. The rigid pole degrees of freedom are all fixed (DOFs = 0). The moving beam and its supports are fixed in all DOFs except for the moving direction.

3. Results and Discussion

Under this section, first the result of the beam test is shown and discussed, and then the final result of the comparison of the existing TWV and the modified model is presented. Finally, the verification method used to check whether the simulation results are reliable is shown.

3.1. Beam Deformation. The deformation values are obtained by measuring the relative displacement from two nodes (one at the right or left end of the beam and the other at the middle of the beam). With this measurement, the value of the deformation graph for different thicknesses of the beam is shown in Figure 11.

This does mean that a beam with less thickness is always better, because more deformation means that there is a probability of intrusion to the vehicle main compartments.

3.2. Beam Energy Absorption. The energy absorption of different thickness of the bumper beam is shown in Figure 12. As we can see from Figure 12, as the thickness of the beam increases from 4.5 mm to 7 mm, the maximum deformation of the beam decreases, and the rate of decrease becomes also less with the increase of thickness. On the other hand, as can be seen in Figure 10, the higher deformation of the beam leads to more absorption of energy of the composite beam. The maximum amount of energy absorbed by the beam is reduced as the thickness becomes increased.

3.3. Impact Force. The maximum impact force between rigid pole and side bumper beam increased with the increase in thickness of the beam. It is obvious that with an

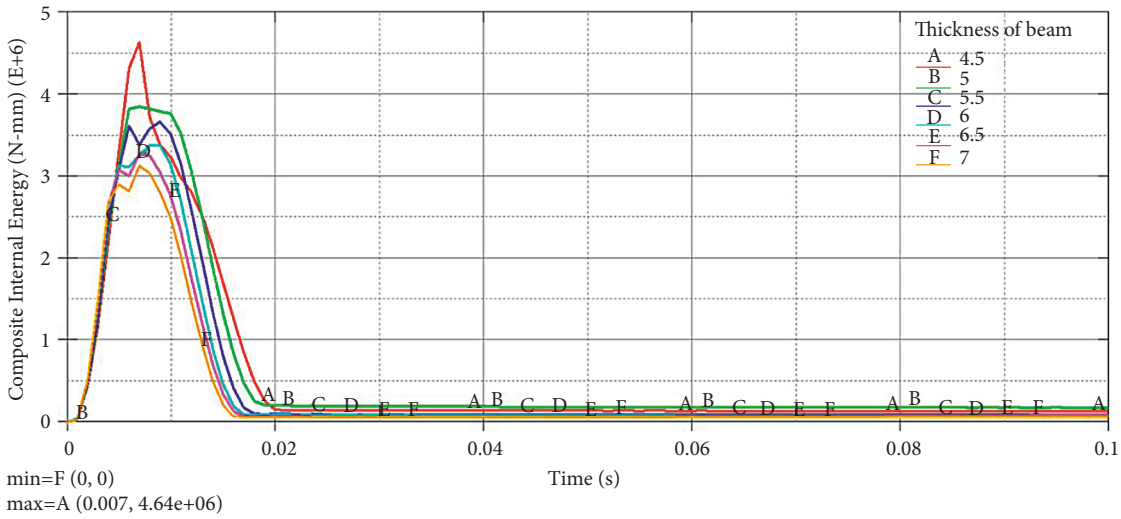

Figure 12: Internal energy of different thicknesses.

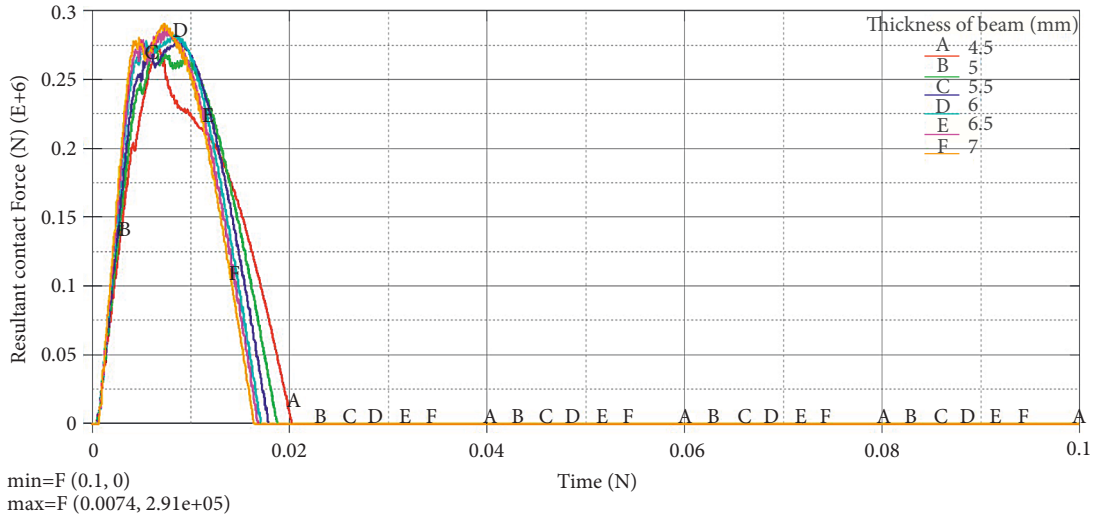

Figure 13: Contact force.

increase in thickness, the mass of the beam increases as a result; the high impact force is produced as shown in Figure 13. But this does not mean that a beam with a smaller thickness is better because the stress on the beam increases with the use of less thickness. Therefore, from the above results, and literature observations it can be concluded that neither a beam with less thickness nor one with higher thickness is better; instead, it depends on the application it is required for [21]. The main purpose of this investigation is to select a lightweight side bumper beam without sacrificing the impact behavior. From the perspective of impact performance, taking the average value for the specified thicknesses improves the level of performance in comparison to other for the TWV's body sections and passengers. Therefore, the bumper beam with 6 mm thickness is better. The von Mises equivalent stress and displacement graph of the selected beam are shown in Figures 11 and 12.

3.4. Effective von Mises Stress. As is indicated in Figure 14, the maximum stress value is equal to 3781 MPa. The composite material strength and failure criteria are determined based on the Chang-Chang failure criterion. If the failure has occurred in all of the laminate layers, then the element will be deleted [22]. Since no dilatation of element was reported when running the simulation, based on that assumption, the beam is safe.

3.5. Resultant Displacement. As is indicated in the counterplot, the maximum resultant deformation of the beam is 32 mm at node 9479. Deformation of the bumper produces changes in the energy absorption of the beam. With this deformation, the intrusion is very much less, and the force of impact is gradually increased, but the damage will be less as compared to the existing one; see Figure 15.

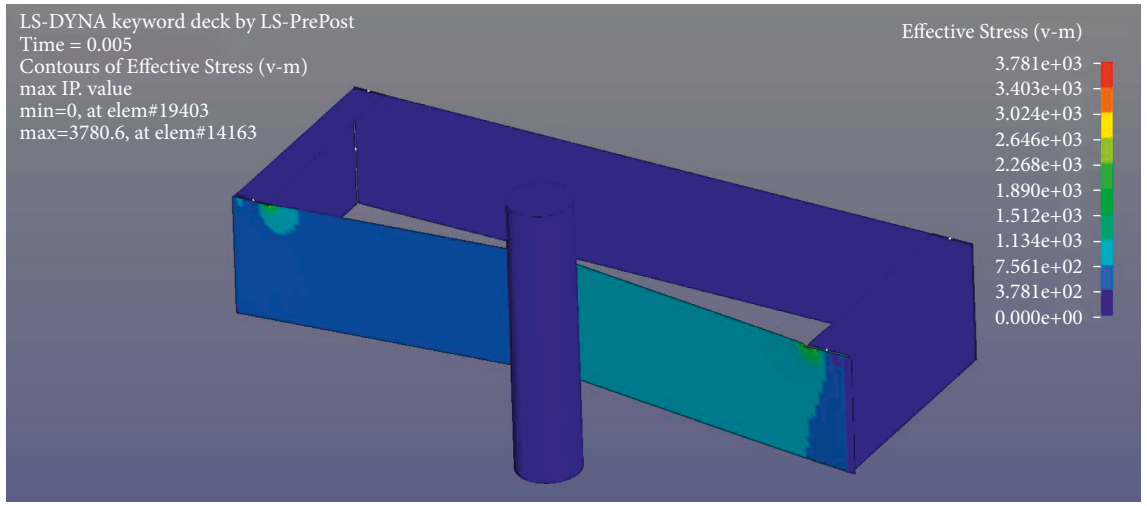

Figure 14: von Mises stress.

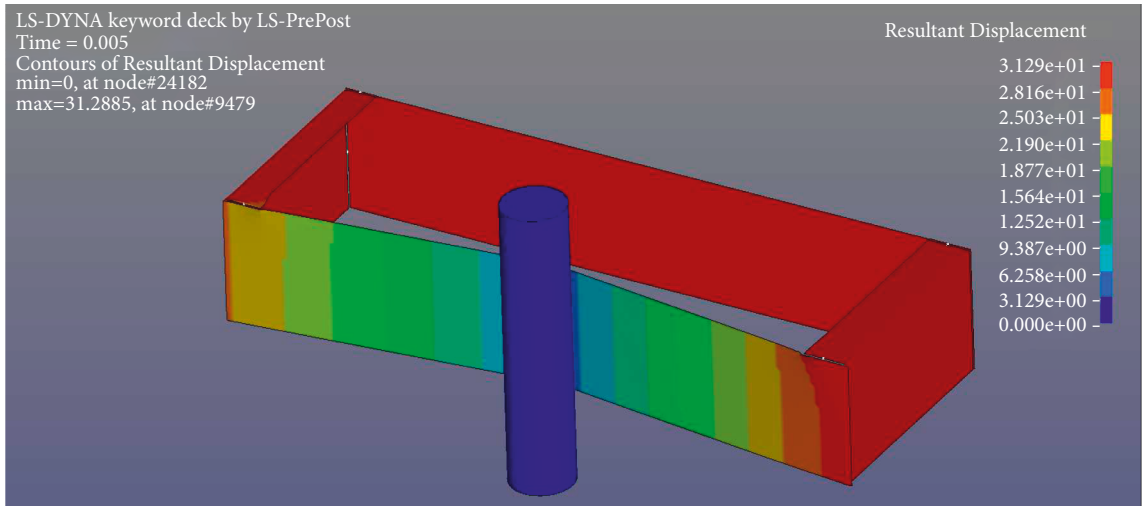

Figure 15: Resultant displacement.

3.6. Dummy and Structure Response. The overall sequence of events during a side impact is shown in Figure 16. The figure shows the response of the structure and the occupants to the side pole collision. The vehicle and its occupants begin to move sideways as the collision process begins. The whole process takes 0.1 s; at initial stages, only small deformation of vehicle and movement (like neck, leg, and shoulder) of occupants is observed until the time reaches 0.45 s. After this point, the force of impact increases as contact between the vehicle and pole increases; as a result, the occupants and the body of the car begin to react in tandem with the occupants' visual movements.

Damage of vehicle body is observed at $t = 0.6$ s. Then, when the time reaches 0.075 s, significant damage to the rear and front structure, roof supports, and lower support is observed, and thus TWV body in addition to the structure is distorted too much, and the occupants start to move toward the side pole. As a result, due to the lack of side doors and the passenger initially positioned on the opposite side of the pole advancing toward the pole, the driver of the TWV falls out of the vehicle as shown in Figure 17 and this shows that when TWV is occupied with three passengers, there is high probability of collision of the passengers with each other and the risk of injury increases as well. At the final stage of the simulation ($t = 0.1$ s), the vehicle is no more protecting the driver from external objects; as a result, the driver slides out of the vehicle and hits the pole. This results in a high degree of injury to the driver body especially around its shoulder, and the passenger also makes a complete circuit of the space through the compartment. This means that any one of the passengers has the probability to be thrown away from the vehicle, which will result in a more severe condition.

As can be observed in Figure 16, the legs of both the driver and passengers are on the twisted position.

This results in serious injuries of the legs, and the force of the necks and shoulders will also put them at higher risk. Figure 16 shows the contact area deformed position and critical points of the occupants during the collision process.

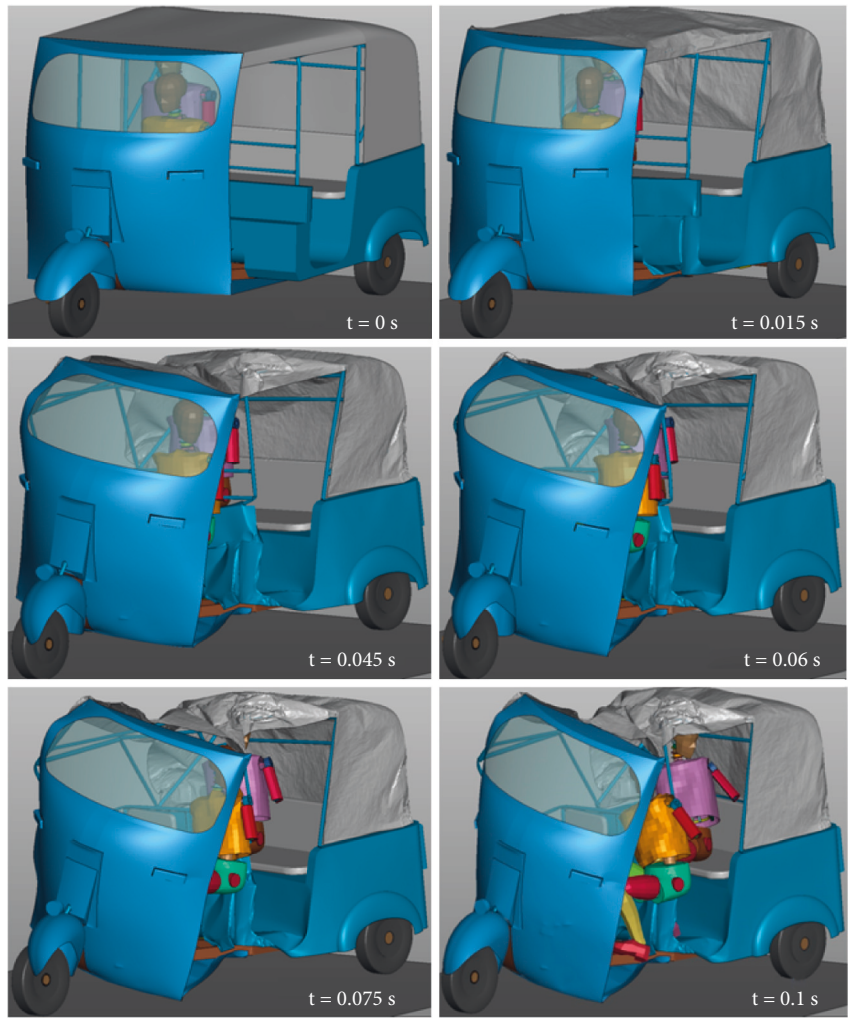

Figure 16: Side crash sequence.

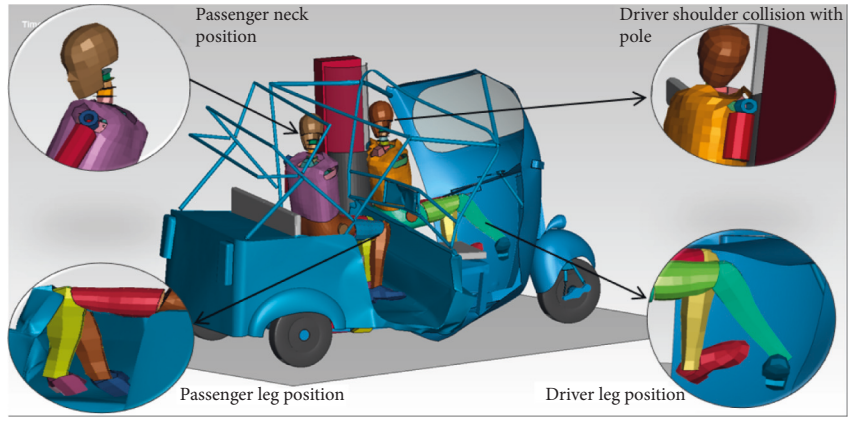

Figure 17: Occupant contact area with TWV.

3.7. Structural Response. Figure 18 shows the structural response of the existing and modified TWV for 0.1 s.

The parameter used to compare the structural response is the occupant's living space remaining after collision. Figure 18(a) shows the space remaining for the existing model and Figure 18(b) shows the modified one. The pole intrudes 320 mm in the case of an existing model and 253 mm in the case of a modified one. The original lateral spacing of the model before the collision is 1250 mm. Subtracting the intruding distance from the original width will give a remaining space of 930 mm and 997 mm for the existing and modified TWV model, respectively. This shows

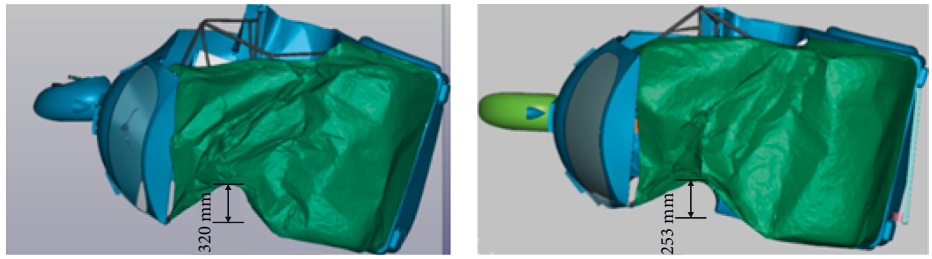

(a) (b)

Figure 18: TWV structural response: (a) existing and (b) modified.

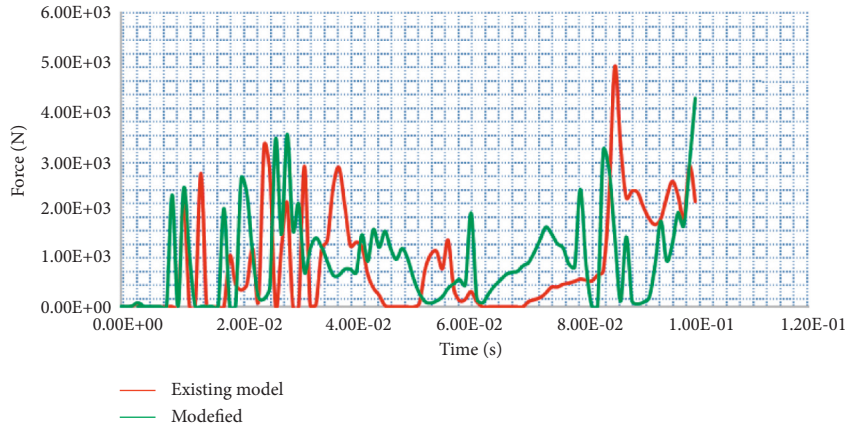

Figure 19: Force of impact.

that the modified model has remained with more living space after the side pole collision.

3.8. Force of Impact. The contact force between the TWV and the rigid pole is shown in Figure 19. The red line indicates the existing model, and the green one shows the modified model force of impact.

As is shown in the graph, the maximum impact force occurs at the existing model with a value of 4870 N. The force on the modified model is equal to 4240 N, and their difference equals 630. This much difference in force can create more momentum to the vehicle; as a result, the vehicle is highly damaged. The higher force of impact may cause more damage to the passengers and the driver. So it can be concluded that the modified model will decrease the impact force on the driver as well as the occupants.

3.9. Energy Absorption. The absorption ability of the modified and existing model is shown in Figure 20. Since the same conditions are applied in the simulation of both models, the energy absorption capacity of the models is determined by using the total internal energy graph.

The model internal energies are shown with green (modified) and red lines (existing). As is indicated in the graph, a maximum amount of kinetic energy is absorbed in the case of the modified model.

With a value equal to 11 kJ of internal energy, the existing model remains with 10.2 kJ. This shows that for the same condition, the modified model can absorb more kinetic energy with less deformation. This helps in reducing the energy transferred to the occupants of TWV.

3.10. Verification Parameters. With the absence of experimental data, the appropriateness of the values obtained on computer simulations can be cheeked by the verification process. In the case of LS-DYNA simulation, verification can be made [23]. The most common and logical ways are listed as follows:

(i) Energy ratio

(ii) Ratio of TE/HE

3.11. Deformation. The deformation results from the existing and modified model are shown in Figure 21. The red line shows the displacement of the existing TWV, and the green line indicates the modified model. The maximum deformation for the existing model and modified model is equal to 345 mm and 286 mm, respectively. It is clear that the maximum deformation occurs in the existing model. For the modified model, the maximum deformation occurs earlier at 0.055 s and decreases, whereas in the case of the existing model, the deformation increases linearly. This shows that there is a reduction in energy in the duration of 0.1 s for the modified model.

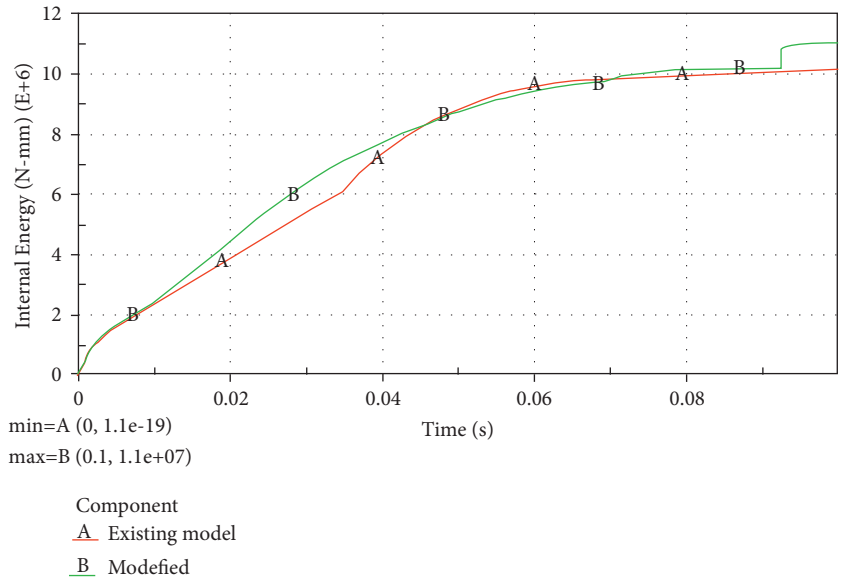

Figure 20: Energy absorbed.

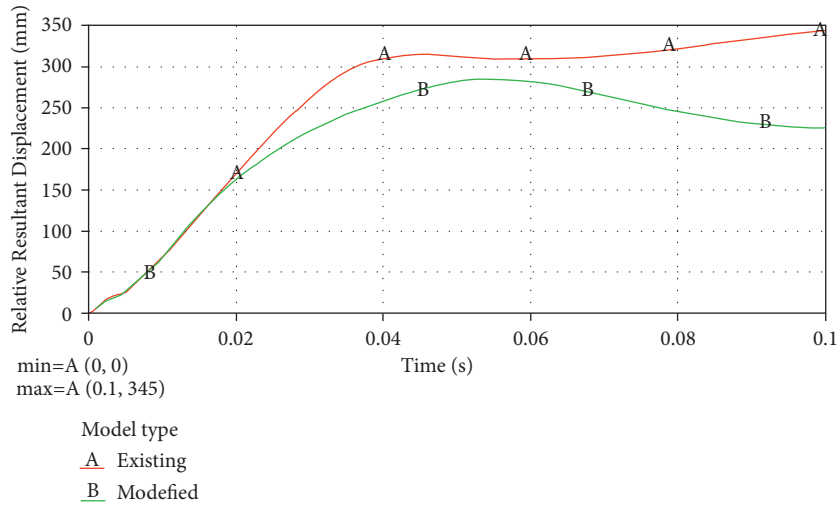

Figure 21: Deformation.

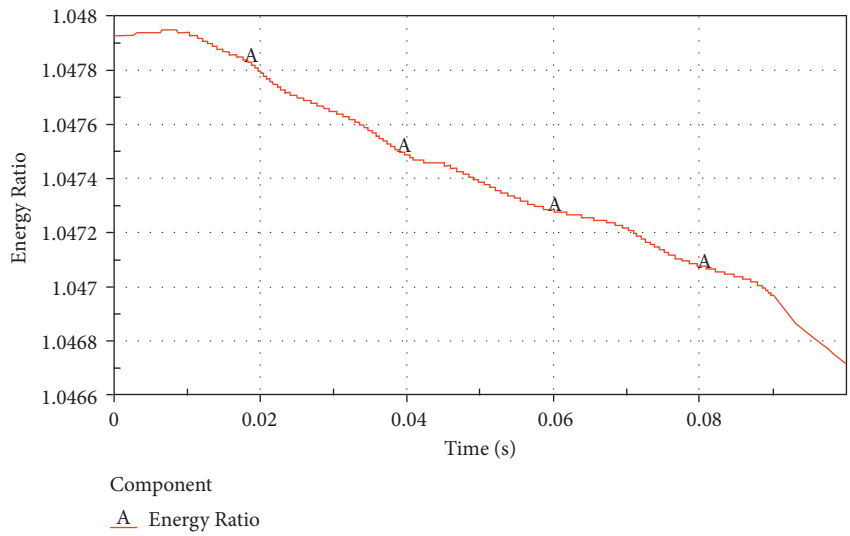

Figure 22: Energy ratio.

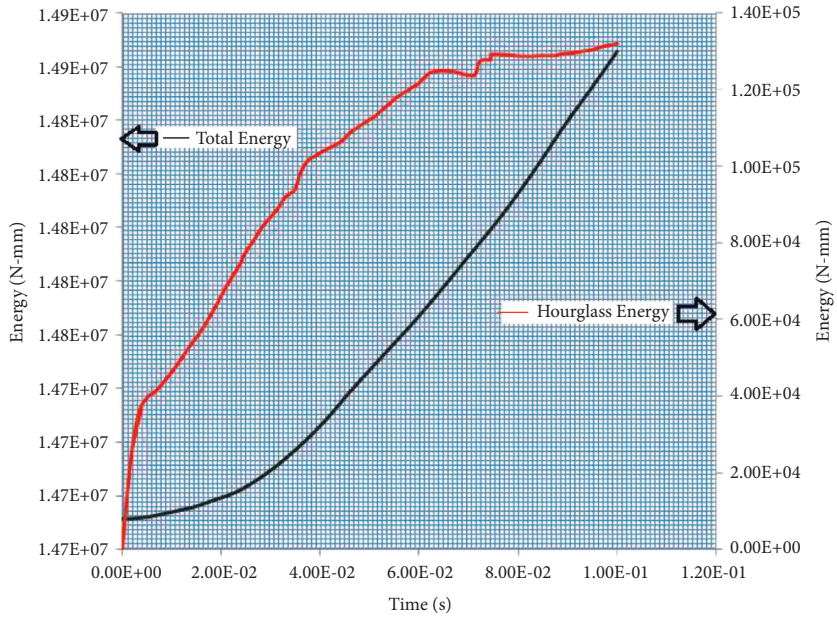

Figure 23: Ratio of HE/TE.

3.12. Energy Ratio. As can be seen in Figure 22, for the 0.1 s simulation, the energy ratio value varies between 1.048 and 1.0466. Since the energy ratio value is acceptable if it is in the range of 1.00 ± 0.07 [23], the indicated value is acceptable.

3.13. The Ratio of HE/TE. In addition to the energy ratio, the energy curves of the finite element model can be validated using the ratio between the total energy and the hourglass energy. Hourglass energy can cause a zero-energy model.

If the hourglass energy is less than 5% of the total energy, the finite element model is reliable [23]. As we can see from Figure 23, the hourglass curve is much lower than that of total energy, or in other words the ratio is less than 5%.

4. Conclusions

This paper establishes the FEA model of an auto-rickshaw to improve the side crashworthiness of existing TWV through dynamic impact simulations. This study clearly shows the simulation of TWV in an event of a side crash. It also shows the occupant response during the collision process. Thus, the existing standards and regulations are used to computationally analyze the crashworthiness. In addition, based on the results obtained from the existing model, an attempt was made to modify the structural crashworthiness of the TWV. As a result, the modified TWV has improved side crashworthiness features. Key findings are summarized as follows:

(i) The structure of the modified model has produced more living space than that of the existing model by only deforming 250 mm whereas the existing model deformed 320 mm. This shows that in an event of side collision, the modified model provides more protection to the occupants and the vehicle sensitive parts.

(ii) The force produced due to the collision of the vehicle into the pole is less for the modified model. A reduction of 630°N force was obtained by the implementation of the modifications. The reduction of contact force resulted in a reduced rate of transferred impact energy to the occupants.

(iii) The modified model also absorbs more energy than the existing model. It absorbed additional 0.8 kJ energy.

Data Availability

The data used to support the findings of this study are included within the article.

Conflicts of Interest

The authors declare that there are no conflicts of interest.

References

[1] V. H. Mohammad, *Evaluation of New Steel and Composite Beam Designs for Side Impact Protection of a Sedan as Per FMVSS 214, IIHS and Side Pole Tests Requirements*, Osmania University, Hyderabad, India, 2010.

[2] E. Nassiopoulos and J. Njuguna, "Finite element dynamic simulation of whole rallying car structure: towards a better understanding of structural dynamics during side impacts," in *Proceedings of the 8th European LS-DYNA Users Conference*, Strasbourg, France, May 2011.

[3] D. Wang, G. Dong, J. Zhang, and S. Huang, "Car side structure crashworthiness in pole and moving deformable barrier side impacts," *Tsinghua Science and Technology*, vol. 11, no. 6, pp. 725–730, 2006.

[4] N. D. Misal, B. P. Ronge, and M. M. Gore, "A review paper on design and analysis of the system of three-wheeler,"

International Journal of Application or Innovation in Engineering & Management, vol. 4, 2015.

[5] K. M. Srikanth and R. V. Prakash, "Assessing the structural crashworthiness of a three-wheeled passenger vehicle," in *Proceedings of the 2nd International Conference on Research into Design*, pp. 152–159, Bangalore, India, September 2009.

[6] A. Sheldon, *IIHS Side Impact Parametric Study Using LS-DYNA® Reichert*, 15th International LS-DYNA Users Conference, Detroit, MI, USA, 2018.

[7] B. Eromo, *School of Mechanical, Chemical, and Material Engineering Improvement of Structure and Body of Three Wheeler Vehicle A Thesis Submitted in Partial Fulfillment of the Requirements for the Award of the Degree of Master of Science in Automotive Engineering*, Adama Science and Technology University, Adama, Ethiopia, 2017.

[8] D. Enawgew, "Strength analysis of three-wheeled vehicle's chassis and body frame assembled in ethiopia by a thesis submitted to school of mechanical and industrial engineering presented in partial fulfillment," M Sc. thesis, Addis Ababa Institute of Technology, Addis Ababa, Ethiopia, 2013.

[9] A. Chawla, S. Mukherjee, and D. Mohan, *Impact Biomechanics in Two Wheeled and Three Wheeled Vehicles*, Indian Institute of Technology, New Delhi, India, 2001.

[10] A. Chawla, S. Mukherjee, D. Mohan, J. Singh, and N. Rizvi, *Crash Simulations of Three-Wheeled Scooter Taxi (Tst)*, Indian Institute of Technology, New Delhi, India, 1997.

[11] M. A. Kunle, M. J. Farah, A. Ahmed, and Mohamed, "Auto rickshaw impacts with pedestrians - a computational analysis of post- collision kinematics and injury mechanics a thesis submitted to cardiff university for the degree of doctor of philosophy," Cardiff University, Cardiff, Wales, Doctor of Philosophy, 2019.

[12] S. Ragul, S. Siddeswaran, and H. Sankarasubramanian: The Validation of Auto Rickshaw Model for Frontal Crash Studies Using Video Capture Data. No. 2020-28-0490. SAE Technical Paper, 2020.

[13] NHTSA (n.d.), "Crash simulation vehicle models | NHTSA," https://www.nhtsa.gov/crash-simulation-vehicle-models.

[14] H. Singh and I. Edag, *Mass Reduction For Light-Duty Vehicles For Model Years 2017–2025 Final Report*, National Highway Traffic Safety Administration, Washington, DC, USA, 2012.

[15] S. Mankar, "Comparative evaluation of steel and composite side impact beams at low-speed impact," *International Journal of Engineering and Techniques*, vol. 4, no. 5, pp. 57–61, 2018.

[16] T. Wang and Y. Li, "Design and analysis of automotive carbon fiber composite bumper beam based on finite element analysis," *Advances in Mechanical Engineering*, vol. 7, no. 6, Article ID 168781401558956, 2015.

[17] S. Mahadevan and X. Liu, "Optimization of composite structures for reliability requirements," *6th Symposium on Multidisciplinary Analysis and Optimization*, American Institute of Aeronautics and Astronautics, Reston, VI, USA, pp. 162–167, 1996.

[18] B. Wade and P. Feraboli, "LS-DYNA MAT54 modeling of the axial crashing of composite fabric channel and corrugated section specimens," *FAA JAMS 2014 Technical Review Meeting*, vol. 37, 2014.

[19] LSTC, "Modeling of composites in LS-DYNA," 2012, http://ftp.lstc.com/anonymous/outgoing/jday/composites/mat_comp.pdf.

[20] D. H. Basavaraju, "Design and Analysis of a Composite Beam for Side Impact," *International Research Journal of Engineering and Technology*, vol. 3, 2005.

[21] Y. Hu, C. Liu, J. Zhang, G. Ding, and Q. Wu, "Research on carbon-fiber-reinforced plastic bumper beam subjected to low-velocity frontal impact," *Advances in Mechanical Engineering*, vol. 7, no. 6, Article ID 168781401558945, 2015.

[22] S. K. Krishnamoorthy, "Prediction of Structural Response of FRP Composites for Conceptual Design of Vehicles under Impact Loading," in *Proceedings of the 8th European LS-DYNA Conference*, 23.-24. Mai, Frankreich, 2011.

[23] O. Gulavani, K. Hughes, and R. Vignjevic, "Explicit dynamic formulation to demonstrate compliance against quasi-static aircraft seat certification loads (CS25.561) -Part I: influence of time and mass scaling," *Proceedings of the Institution of Mechanical Engineers - Part G: Journal of Aerospace Engineering*, vol. 228, no. 11, pp. 1982–1995, 2014.